Proceedings of the Jangjeon Mathematical Society
24 (2021), No. 4, pp. 569 – 582

www.jangjeon.or.kr
http://dx.doi.org/10.17777/pjms2021.24.4.569

USE OF QUANTUM MECHANICAL FRAGMENTATION APPROACH IN DECAY DYNAMICS OF ^{221}FR NUCLEUS

MANOJ K. SHARMA AND AMANDEEP KAUR

Abstract. The ground state and excited state decay dynamics of ^{221}Fr nucleus is studied using the quantum mechanical fragmentation theory (QMFT) based methodology. The decay paths of ground state ^{221}Fr nucleus, i.e. α-decay, cluster emission and spontaneous fission (SF), are explored within the preformed cluster model (PCM). The relative contribution of these decay modes is investigated in terms of fragmentation potential and preformation probability P_0. The calculations are made for the spherical as well as deformed choice of decaying fragments. Here, the deformation effects are included upto quadrupole (β_2) shapes of nuclei with 'hot-compact' and 'cold-elongated' optimum orientations. The half-life times ($T_{1/2}$) of α particle and ^{14}C cluster are calculated using β_2-deformed fragmentation, and find reasonable agreement with the experimental data. The spontaneous fission decay fragments are identified for ^{221}Fr parent nucleus and corresponding decay half-life time is predicted. Further, the excited state decay of ^{221}Fr* compound nucleus formed in ^{19}F+^{202}Pt reaction is studied at excitation energy E^*_{CN}=10 MeV within the framework of the dynamical cluster-decay model (DCM). Note that DCM is an extended version of PCM, where temperature (T) and angular momentum (ℓ) are duly incorporated. The evaporation residue (ER) and fusion-fission (ff) cross-sections are calculated using hot-compact fragmentation approach. Finally, a relative study of spontaneous fission and induced fission is presented in terms of barrier characteristics and potential energy surfaces.

2010 Mathematics Subject Classification. 81T23, 00A72.

Keywords and phrases. α-decay, cluster decay, spontaneous fission, induced fission.

1. Introduction

Numerous theoretical/computational techniques have been formulated to understand the dynamics associated with the decay of nuclear systems. Such techniques call forth the innovative thinking and new philosophies in addressing different type of nuclear processes. The motive of this work is to highlight some analytical and computational methods employed to analyze the dynamics associated with ground state and excited state nuclear systems. The main driving factors relating to these processes are: structure, mechanism and energy dissipation etc., which affect the decay dynamics of nuclear entities. Based on quantum mechanical fragmentation theory (QMFT) [1], which considers mass (or charge) asymmetry coordinate as a dynamical coordinate to study the mass (or charge) transfer in a nuclear decay process, two approaches such as preformed cluster model (PCM) [2, 3, 4] and dynamical cluster-decay model (DCM) [5, 6, 7] have been established over last few decades. The PCM approach is utilized to analyze the ground state decay mechanisms, for example α-decay [2], cluster radioactivity (CR) [4] and spontaneous fission (SF) [3]. The

Submitted on November 25, 2019.

most prominent decay mode in heavy radioactive nuclear systems is α-decay, which was identified as a ^{4}He-emission in 1907 [8]. Whereas, the spontaneous fission process was discovered in 1940 by two Russian physicists (G. Flerov and K. Petrzhak) by dividing Uranium nucleus into two smaller nascent fragments [9]. Apart from these decay modes, the ground decay process of cluster radioactivity was observed experimentally from ^{223}Ra radioactive nucleus in 1984 [10]. In this phenomenon, the radioactive nucleus is assumed to decay into a cluster, which is larger than the α-particle but smaller than the lightest of fission fragments.

The DCM approach is focused on the decay of excited and rotating projectile-target (P-T) composite system formed in light and heavy-ion induced reactions. Depending on various reaction conditions, the P-T composite system may decay via various compound nucleus (CN) and/or non-compound nucleus (nCN) processes. The comprehensive analysis of CN (evaporation residue (ER) and fusion-fission (ff)) and nCN (quasi fission, fast fission and deep inelastic collision) processes has been carried out in terms of various observables of DCM such as fragmentation potential, preformation probability, barrier penetrability and decay cross-sections etc [5]. In both approaches (i.e. PCM and DCM), the combine effect of attractive and repulsive potentials is examined in terms of collective fragmentation potential, which is calculated using Strutinsky macro-microscopic method [11]. The fragmentation potential goes as input to the Schrodinger equation, and further solved to estimate the preformation probability (P_0) of the decaying fragments. The preformation probability determines the fragment mass distributions and in turn help to identify the energetically favored nascent fragments. Interestingly, both PCM and DCM computational techniques follow the collective clusterization method which treats all the decay processes on parallel footing. Note that this aspect of handling different decay processes in unique set of calculation is not available in majority of competing models.

In the present work, the ground state and excited state decay processes for ^{221}Fr nucleus are investigated within PCM and DCM, respectively. The relative contribution of different ground state decay modes such as α-decay, cluster-emission and spontaneous fission, and their corresponding decay half-life times are evaluated within the PCM. It is important to note that the shapes of fragments and their orientations play important role in the decay dynamics. Therefore, the relative influence of spherical and deformed fragmentation is investigated in view of decay products and their half-life times. The deformation effects are included up to quadrupole β_2 shapes of decaying fragments with 'optimum' orientations ($\theta_i^{opt.}$). Where, orientations are optimized based on the sign of β_2, which further characterizes the 'hot-compact' or 'cold-elongated' configuration [13].

To study the excited state decay mechanism such as evaporation residue (ER) and fusion-fission (ff) ('or' say induced fission), the compound nucleus ^{221}Fr* is chosen, which is formed in ^{19}F+^{202}Pt reaction at excitation energy E^{*}_{CN}=10 MeV. The excited state decay calculations are made for the β_2-deformed nuclei with hot-compact configurations within the framework of dynamical cluster-decay model (DCM). The fragmentation decay path is investigated to see the relative contribution of ER and fission channels. Further, a comparative study of spontaneous fission and fusion-fission is carried out in terms of scattering potential and fragmentation potential. In the following section, the illustration of quantum mechanical fragmentation theory based PCM and DCM methods is given.

2. Methodology

2.1. **Quantum mechanical fragmentation theory.** The quantum mechanical fragmentation theory (QMFT) investigates the mass and charge transfer in a nuclear decay process by considering mass asymmetry ($\eta_A = (A_1 - A_2)/(A_1 + A_2)$) and charge asymmetry ($\eta_Z = (Z_1 - Z_2)/(Z_1 + Z_2)$) as a dynamical collective coordinates. Apart from these asymmetry coordinates, the shape of nucleus is defined by following coordinates: (i) relative separation R between the two nuclei (ii) deformations $\beta_{\lambda i}$ and orientations (θ_i) of two nuclei, where i=1,2 and λ=2,3,4... (iii) the neck parameter, and (iv) azimuthal angle ϕ between principal planes of interacting nuclear systems. The pictorial view of two deformed nuclei lying in the same plane (i.e. ϕ=0), can be seen in Fig. 2 of ref. [12].

The structure information of decaying nucleus is extracted from the fragmentation potential $V_R(\eta,T)$, which is calculated in terms of collective coordinates, and written as

$$\begin{aligned} V_R(\eta,T) = &\sum_{i=1}^{2}[V_{LDM}(A_i,Z_i,T)] + \sum_{i=1}^{2}[\delta U_i]exp(-T^2/T_0^2) \\ &+V_C(R,Z_i,\beta_{\lambda i},\theta_i,T) + V_P(R,A_i,\beta_{\lambda i},\theta_i,T) \\ &+V_\ell(R,A_i,\beta_{\lambda i},\theta_i,T). \end{aligned} \tag{1}$$

V_{LDM} is the T-dependent liquid drop energy of Davdison *et al.* [14] with its constants at T=0 re-fitted in Refs. [15, 16] to give the experimental binding energies of Audi *et. al.* [17] or that of Moller *et al.* [18], wherever not available in [17]. δU, the "empirical" shell correction [19], also made T-dependent [20]. V_C, V_P and V_ℓ are respectively, the T-dependent Coulomb, the nuclear proximity and centrifugal potentials for deformed and oriented nuclei [16].

Using fragmentation potential $V_R(\eta,T)$, the preformation yields $P_0(A_i)$ of decaying fragments (A_i) is obtained by solving the Schrödinger equation in η-coordinate at fixed $R = R_a$ (the entry point of penetration path),

$$\left\{-\frac{\hbar^2}{2\sqrt{B_{\eta\eta}}}\frac{\partial}{\partial\eta}\frac{1}{\sqrt{B_{\eta\eta}}}\frac{\partial}{\partial\eta} + V_R(\eta,T)\right\}\psi^\nu(\eta) = E^\nu\psi^\nu(\eta), \tag{2}$$

with $\nu = 0, 1, 2, 3...$ referring to ground state ($\nu = 0$) and excited state solutions, with the ground state preformation probability P_0 given as

$$P_0 = |\psi(\eta(A_i))|^2\sqrt{B_{\eta\eta}}\frac{2}{A_{CN}}, \tag{3}$$

The higher values of ν contribute to the excited states, and these contributions enter via excitation of higher vibrational states. The wave function for such excited states, is given by

$$|\psi|^2 = \sum_{\nu=0}^{\infty}|\psi^\nu|^2 exp(-E^\nu/T). \tag{4}$$

P_0 is the probability of finding certain mass fragments at position R on the decay path and $B_{\eta\eta}$ represents the smooth hydrodynamical mass parameter [21].

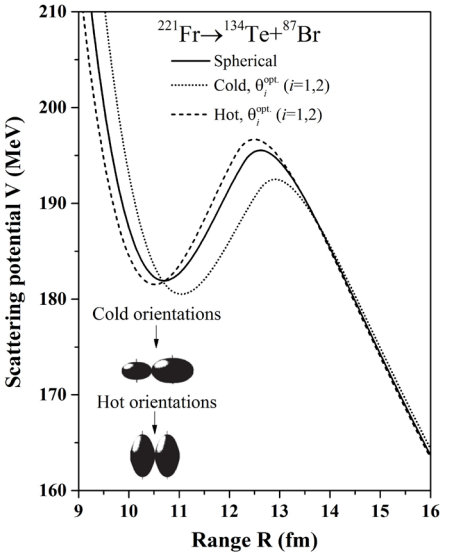

FIGURE 1. The scattering potential V(R) illustrated for the spontaneous fission decay of ^{221}Fr nucleus calculated for spherical (solid line), and β_2-deformed choice of fragmentation with optimum orientation (θ_i) forming hot compact (dashed line) and cold elongated (dotted line) configuration.

After determining the preformation probability of decaying fragments, the penetration probability P of decaying fragments is calculated using Wenzel-Kramers-Brillouin (WKB) integral,

$$P = exp[-\frac{2}{\hbar}\int_{R_a}^{R_b}\{2\mu[V(R) - Q_{eff}]\}^{1/2}dR] \tag{5}$$

with $V(R_a, T) = V(R_b, T) = TKE(T) = Q_{eff}(T)$ for the two turning points. $V(R_a, T)$ acts like an effective Q value of decay, $Q_{eff}(T)$, and $TKE(T)$ as the total kinetic energy of decaying fragments. The entry point of penetration path, R_a is defined as

$$\begin{aligned} R_a(T) &= R_1(\alpha_1, T) + R_2(\alpha_2, T) + \Delta R(T) \\ &= R_t(\alpha, T) + \Delta R(T), \end{aligned} \tag{6}$$

with radius vectors R_i $(i = 1, 2)$

$$R_i(\alpha_i, T) = R_{0i}(T)\left[1 + \sum_{\lambda}\beta_{\lambda i}Y_{\lambda}^{(0)}(\alpha_i)\right] \tag{7}$$

and T-dependent nuclear radii R_{0i} of the equivalent spherical nuclei [22],

$$R_{0i}(T) = [1.28A_i^{\frac{1}{3}} - 0.76 + 0.8A_i^{\frac{-1}{3}}](1 + 0.0007T^2)fm. \tag{8}$$

The only parameter of the model is termed as neck-length parameter (ΔR), which assimilates the neck formation effects. Apart from this, the choice of best fitted ΔR allows us to define the 'barrier lowering' parameter ΔV_B as a function of ℓ, as

$$\Delta V_B(\ell) = V(R_a, \ell) - V_B(\ell). \tag{9}$$

Here, $V(R_a, \ell)$ and $V_B(\ell)$ are the actual barrier used and the top of barrier, respectively.

In DCM, the compound nucleus (CN) decay cross-sections are calculated in terms of ℓ-partial waves using the decoupled approximation to R and η motions

$$\sigma(A_1, A_2) = \frac{\pi}{k^2} \sum_{\ell=0}^{\ell_{max}} (2\ell + 1) P_0 P; \quad k = \sqrt{\frac{2\mu E_{c.m.}}{\hbar^2}}, \tag{10}$$

where P_0 and P are calculated using Eqs. (3) and (5), which depend on the CN excitation energy, deformations and orientations of fragments. The maximum angular momentum (ℓ_{max}) is fixed for the vanishing of the light particles cross-section i.e. $\sigma_{ER} \to 0$, and μ ($=A_1 A2/(A_1 + A_2)$) is the reduced mass.

In PCM approach, the decay half-life ($T_{1/2}$) is calculated as

$$T_{1/2} = \frac{ln2}{\lambda}, \quad \lambda = \nu_0 P_0 P. \tag{11}$$

Here, ν_0 is the barrier assault frequency, and reads as

$$\nu_0 = \frac{velocity}{R_0} = \frac{(2E_2/\mu)^{1/2}}{R_0}, \tag{12}$$

It is important to note here that PCM is the temperature independent version (i.e. T=0) of DCM. The P_0 is calculated using equation (3) for ground state. However, in PCM, penetration probability is calculated in three steps, as shown in Fig. 7: (i) the penetrability P_a from R_a to R_i with $V(R_a) = V(R_i)$, (ii) the de-excitation probability W_i at R_i, and taken as unity, refer Ref. [23], and (iii) the penetrability P_b from R_i to R_b, with V(R_b)=Q_{out}, giving

$$P = P_a W_i P_b \tag{13}$$

where P_a and P_b are the WKB integrals, for details see Ref. [2].

3. Calculations and discussions

This section is divided into three sub-sections, and reveals interesting aspects associated with the dynamics of ground state and excited state decays of ^{221}Fr nucleus. First of all, section 3.1 represents the ground state decay paths of ^{221}Fr nucleus, which are studied using PCM method. The influence of deformations as well as orientations of decaying fragments is analyzed in terms of barrier characteristics, fragmentation potential and fragment mass distributions. Moreover, the half-life times are calculated for α-decay, cluster and spontaneous fission decay modes, and the results are compared with the available experimental data. The excited state decay dynamics of ^{221}Fr* compound nucleus (CN) formed in ^{19}F+^{202}Pt reaction is discussed in section 3.2. The evaporation residue (ER) and fusion-fission (ff) processes of ^{221}Fr* are studied within DCM approach. Finally, a comparative analysis of ground state fission and induced fission is made in section 3.3.

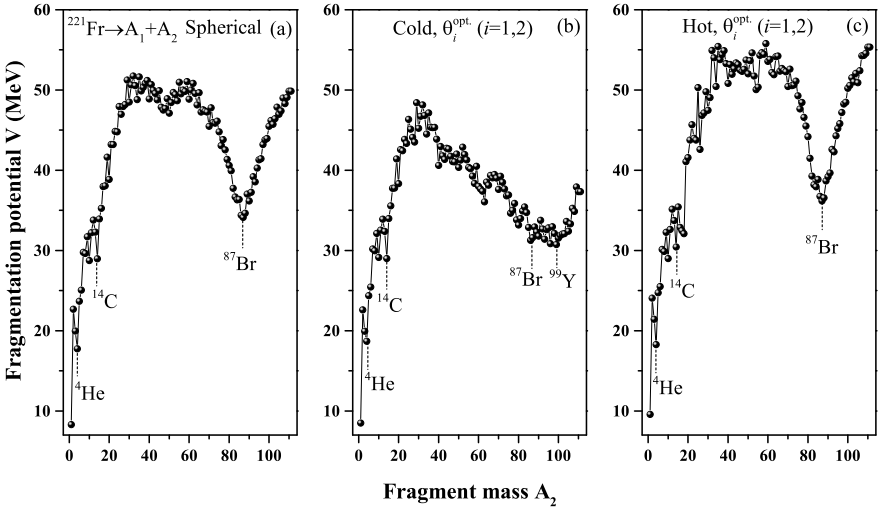

FIGURE 2. Variation of fragmentation potential V(MeV) as a function of fragment mass (A_2) for ^{221}Fr nucleus. Results are shown for (a) spherical, (b) cold-elongated and (c) hot-compact configurations of fragments.

3.1. **Analysis of various ground state decay mechanisms of ^{221}Fr nucleus.** In this section, the spontaneous decay of ^{221}Fr nucleus via alpha (α), cluster (^{14}C) and fission processes is studied. The ground state analysis is carried out within the preformed cluster model (PCM) where temperature (T) effects are silent. The angular momentum effects are included upto ℓ=5$\hbar$ for all the ground state decay processes in view of [2]. Fig. 1 show the interaction ('or' scattering) potential as a function of internuclear separation (R) for the spontaneous fission (SF) decay of ^{221}Fr nucleus for the case of spherical and β_2-deformed choice of fragments. For the choice of β_2-deformations, the optimum orientations θ_i are uniquely fixed on the basis of sign of β_2 [13], which appear in the form of 'hot-compact' and 'cold-elongated' configuration as shown in fig. 1. It is depicted from the figure that the interaction radius decreases and interaction barrier increases as one goes from cold-elongated to spherical to hot-compact configuration. The significant change in the barrier characteristics (barrier height (V_B) and barrier position (R_B)) correspondingly affect the penetration probability (P), and hence the half-life time ($T_{1/2}$).

Figs. 2 (a-c) represent the PCM-calculated fragmentation potential $V_R(\eta,T)$ as a function of fragment mass (A_2) of ^{221}Fr parent nucleus for spherical and quadrupole (β_{2i}) deformed choice of fragmentation. The influence of 'hot-compact' and 'cold-elongated' configurations of orientations for β_{2i}-deformed fragments are also studied in Fig. 2. As discussed in above, the magnitude of interaction barrier is higher for hot-compact configuration than cold-elongated configuration. It is also evident from Fig. 2 that the magnitude of fragmentation potential show increment as one goes from cold-elongated to spherical and spherical to hot-compact choice of configuration. It is noticed that the structure of fragmentation potential is significantly

TABLE 1. PCM-calculated half-life times ($T_{1/2}$) for alpha (^{4}He), cluster (^{14}C) and spontaneous fission (^{87}Br) decays, and compared with available experimental data [24, 25]. The fitted neck-length parameter ΔR and other calculated quantities such as preformation probability P_0 and penetrability P are also presented.

Decay modes	Decay channel	ΔR (fm)	P_0	P	$log_{10}T_{1/2}$ (s) DCM	Expt.
Spherical						
Alpha	^{4}He+^{217}At	0.9	1.09X10^{-9}	2.40X10^{-10}	5.18	2.47
Cluster	^{14}C+^{207}Tl	0.5	1.45X10^{-23}	3.59X10^{-20}	20.8	>13.8
Cold, $\theta_i^{opt.}$ (i=1,2)						
Alpha	^{4}He+^{217}At	0.9	2.40X10^{-10}	3.32X10^{-18}	5.56	2.47
Cluster	^{14}C+^{207}Tl	0.5	3.59X10^{-20}	3.03X10^{-20}	17.3	>13.8
Hot, $\theta_i^{opt.}$ (i=1,2)						
Alpha	^{4}He+^{217}At	1.04	1.94X10^{-9}	1.67X10^{-17}	4.94	2.47
Cluster	^{14}C+^{207}Tl	0.52	1.16X10^{-16}	1.85X10^{-20}	14.0	>13.8
SF	^{134}Te+^{87}Br	0.52	1.0X10^{-38}	2.25X10^{-13}	29.0	-

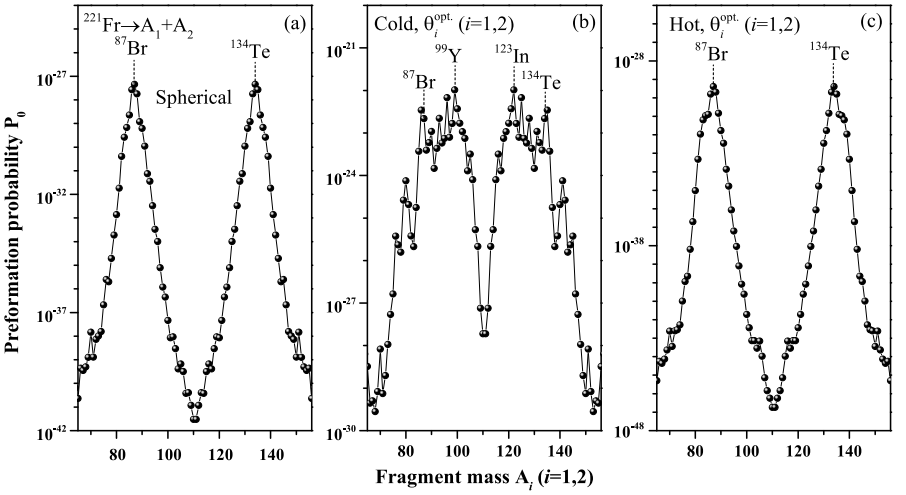

FIGURE 3. The Preformation probability P_0 as a function of fragment mass (A_i; i=1,2) for (a) spherical, (b) cold-elongated and (c) hot-compact choices of configurations.

modified for different choice of orientational configurations. However, independent of deformation effects, the deepest minima of fragmentation potential occurs at same choice of decay fragment(s) such as ^{4}He, ^{14}C and ^{87}Br (plus their complementary

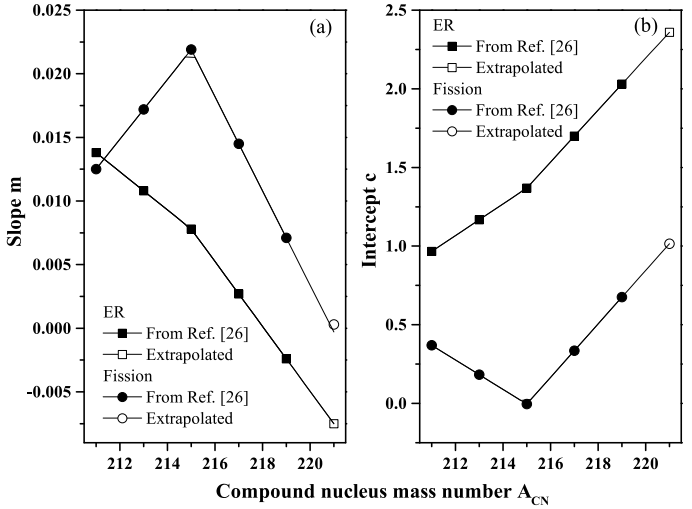

FIGURE 4. (a) Slope and (b) intercept as a function of compound nucleus mass number A_{CN} for straight-line fit of ΔR as a function of E^*_{CN}. Open symbols are extrapolated values and filled symbols are fitted values.

fragments), which means that the emergence of α-decay, cluster emission and spontaneous fission seems evident in the fragmentation structure of ^{221}Fr nucleus. In view of this, we have calculated the decay half-life times of distinct ground state decay paths of ^{221}Fr, for example, alpha (^{4}He), cluster (^{14}C) and spontaneous fission (^{87}Br).

Table 1 show the calculated half-life times ($T_{1/2}$) for alpha (^{4}He), cluster (^{14}C) and spontaneous fission (^{87}Br) decays of ^{221}Fr parent nucleus. The alpha and cluster decay half-lives are calculated by fitting neck-length (ΔR) parameter of the model for all the considered approaches. This parameter assimilates the neck formation effects, and decides the first turning point of the penetration path (see Eq. 6). It is noticed from table that the calculated alpha and cluster decay half-life times for hot-compact configuration show relatively better agreement with the experimental data [24, 25] in comparison with other configurations. The experimental data is available only for the alpha and cluster decay of ^{221}Fr nucleus. Hence, the SF half-life for the decay of ^{221}Fr nucleus is predicted at touching point for the case of hot-compact configurations. Note that all the calculations are made for ℓ=5$\hbar$.

This analysis is carried forward to study the fission fragment mass distributions for the SF decay of ^{221}Fr nucleus. Figs. 3(a-c) depict the preformation probability P_0 as a function of fission fragment mass (A_i) for spherical, cold-elongated and hot-compact choice of configurations. The variation of P_0 remains asymmetric for all three considered choices. However, more structure is seen for the case of cold-elongated configurations of decaying fragments. Interestingly, the choice of most probable decay fragments remain identocal for all three cases. The most probable fragments are marked in Fig. 3.

TABLE 2. DCM-calculated cross-sections for evaporation residue (ER) and fusion-fission (ff) processes of ^{221}Fr* compound nucleus at E^*_{CN}=10 MeV. Other quantities such as neck-length parameter ΔR and maximum angular momentum (ℓ_{max}) are also presented.

Decay channel	ΔR (fm)	ℓ_{max} ($\hbar$)	A_2	σ (mb)
Evaporation residue	2.284	93	1-4	515
Fusion-fission	1.018	113	80-93	0.74

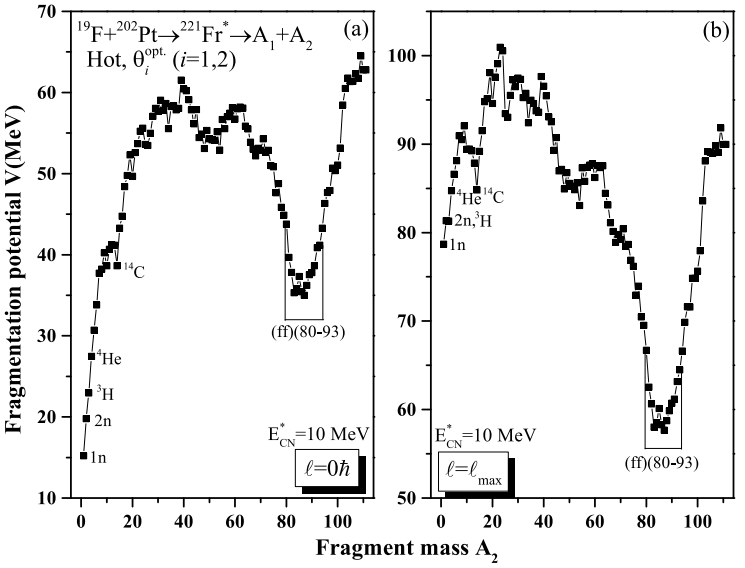

FIGURE 5. The fragmentation potential V (MeV) as a function of fragment mass A_2 for ^{19}F+^{202}Pt→^{221}Fr* reaction illustrated at (a) minimum angular momentum (ℓ_{min}=0$\hbar$), and (b) maximum angular momentum (ℓ_{max}=113$\hbar$).

3.2. **Decay dynamics of ^{221}Fr* compound nucleus formed in ^{19}F+^{202}Pt reaction.** In this section, the excited state decays such as evaporation residue (ER) and fusion-fission (ff) of ^{221}Fr* compound nucleus formed in ^{19}F+^{202}Pt are studied at excitation energy E^*_{CN}=10 MeV. This analysis is carried out within the dynamical cluster-decay model (DCM) for the choice of β_{2i}-deformed fragments with hot-compact configurations. By one of us and collaborators, the decay dynamics of various 'Fr' isotopes with mass number A=211-219 was studied at various excitation energies using DCM approach [26]. The neck-length parameter (ΔR) was extracted as a function of E^*_{CN} are obtained for different isotopes of 'Fr'. Using the systematics of different ΔR values of '$^{211-219}$Fr' isotopes [26], we have extended the study of ER and ff for another francium isotope (^{221}Fr). The values of slope (m) and intercept

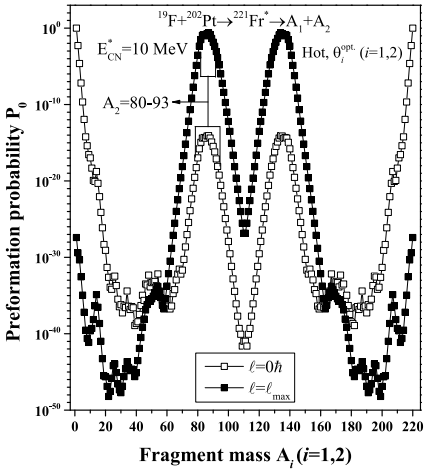

FIGURE 6. Preformation mass yield P_0 as a function of fragment mass for ^{221}Fr* CN at E^*_{CN}=10 MeV, calculated for ℓ=0$\hbar$ and ℓ_{max} value.

(c) are extrapolated which are obtained for the linear fit of ΔR as a function of E^*_{CN} for Fr isotopes using ΔR=mE^*_{CN}+c, as shown in Fig. 4. The obtained linear fits of ER and ff decays for ^{221}Fr nucleus is written as

$$\Delta R^{ER} = -0.0075E^*_{CN} + 2.3596 \quad (14)$$

$$\Delta R^{ff} = 0.0003E^*_{CN} + 1.015. \quad (15)$$

By using above equations the cross-sections for evaporation residue (ER) and fusion-fission (ff) are calculated at E^*_{CN}=10 MeV near the fission barrier are calculated. The calculated cross-sections for ^{221}Fr along with the neck-length parameter ΔR and maximum angular momentum ℓ_{max} are given in table 2.

For further insight, the fragmentation potential of ^{221}Fr* CN is plotted in Fig. 5(a-b) at minimum (ℓ_{min}=0$\hbar$) and maximum (ℓ_{max}=113$\hbar$) angular momentum values. The calculated fragmentation potential signify the relative contribution of different decay channels. It is observed from the figure that the behaviour of fragmentation potential is different at two extreme angular momentum values. At lower angular momentum the light particles are more preferable as compared to other decay channels. However, the heavy fragments such as fission fragments depict a deeper potential energy minimum at maximum angular momentum. This suggests that fusion-fission process is energetically favoured at ℓ_{max}-value. Note that, the fragments for which the fragmentation potential is minimum, possesses the maximum preformation probability. Fig. 6 depicts the preformation probability P_0 as a function of fragment mass for the excited state decay of ^{221}Fr* CN at E^*_{CN}=10 MeV for ℓ_{min} and ℓ_{max} values. The structure of preformation yield depicts the asymmetric fission of ^{221}Fr* compound nucleus. Moreover, the choice of most preferred fission fragments remain identical, independent of the choice of ℓ-values, as marked in the figure.

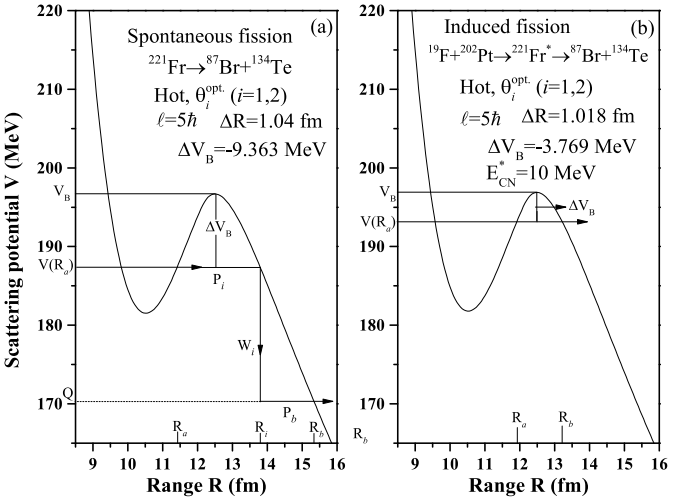

FIGURE 7. The scattering potential V(R) for (a) spontaneous and (b) induced fission of ^{221}Fr nucleus plotted at common ℓ=5$\hbar$.

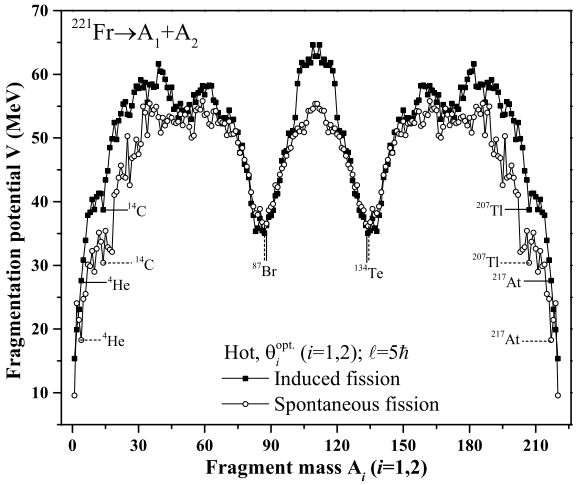

FIGURE 8. The collective fragmentation potential V(MeV) as a function of A_i calculated for spontaneous fission and induced fission of ^{221}Fr at ℓ=5$\hbar$.

3.3. **Relative study of spontaneous fission and induced fission.** This section is focused on the comparative analysis of spontaneous fission and induced fission of ^{221}Fr nucleus. The induced fission is worked out at excitation energy E^*_{CN}=10 MeV and the results are compared with the spontaneous fission which operates at

E=0. As explained in previous two sections, the induced and spontaneous fission are, respectively, studied in DCM and PCM computational methods. The calculations presented in this section are made for the β_2-deformed fragments within hot optimum orientations for both ground and excited state fission processes. To study the barrier characteristics of both processes, Figs. 7(a-b) depict the scattering potential V(R) for spontaneous fission and induced fission at common angular momentum ℓ=5$\hbar$. As shown in figure 7(a), for the case of PCM, the penetration probability P consists of three contributions (i) the penetrability P_i from R_a to R_i, (ii) the (inner) de-excitation probability W_i at R_i, and (iii) the penetrability P_b from R_i to R_b, giving, $P = P_i W_i P_b$. But for the case of fusion-fission it is a single step process as shown in figure 7(b). Though neck-length parameter ΔR is similar for spontaneous and induced fission, corresponding barrier modification (ΔV_B) (in magnitude) is much higher for spontaneous fission as compared to induced fission, possibly because in spontaneous decay, the fragments are in ground state (T=0).

In fig. 8, the fragmentation potential is compared for spontaneous fission and induced fission of ^{221}Fr nucleus at common angular momentum ℓ=5$\hbar$. Both processes depict the similar behavior with respect to the emission of most probable fragments as marked in figure. Note that despite the change in magnitude, the fission valleys in both cases correspond to asymmetric mass fragments which in turn provides us the information concerning the structural aspects in decay of ^{221}Fr nucleus.

4. Summary

We have explored the ground and excited state decay of ^{221}Fr nucleus within the framework of preformed cluster model (PCM) and dynamical cluster-decay model (DCM). These methods are formulated using the quantum mechanical fragmentation theory. In view of the fragmentation analysis the α-decay, cluster (^{14}C) emission and spontaneous fission operate in the ground state decay of ^{221}Fr nucleus. The role of quadrupole deformations and optimum orientations (with 'hot-compact' and 'cold-elongated' configurations) of fragments, is studied in view of fragmentation potential and corresponding impact on the half-life values. The half-life times of α-decay and ^{14}C decay are calculated using best-fit values of neck-length parameter, which show reasonable agreement with the experimental data. Moreover, the distribution of mass fragments for spontaneous fission is observed to be asymmetric. The half-life for the spontaneous fission of ^{221}Fr nucleus is also calculated.

Further, the evaporation residue (ER) and fusion-fission (ff) are investigated within the DCM approach for the excited ^{221}Fr* compound nucleus formed in ^{19}F+^{202}Pt reaction at excitation energy E^*_{CN}=10 MeV. The calculations are made for β_2-deformed fragments with hot-optimum orientations. The contributions of excited state decay paths are evaluated in terms of fragmentation potential and preformation probability. The ER and ff cross-sections are calculated at E^*_{CN}=10 MeV. Finally, the barrier characteristics and decay paths of spontaneous fission and induced fission are compared at common angular momentum values. It is observed that both processes exhibit different barrier characteristics. Although, the structure of the fragmentation potential depicts similar behavior, indicating the asymmetric fission for both processes.

5. Acknowledgement

The financial support from the UGC-DAE Consortium for Scientific Research, F. No. UGC-DAE-CSR-KC/CRS/19/NP09/0920 is gratefully acknowledged.

References

[1] R. K. Gupta, W. Scheid, and W. Greiner, *Theory of Charge Dispersion in Nuclear Fission*, Phys. Rev. Lett. 35 (1975), 353.
[2] K. Sharma, G. Sawhney, and M. K. Sharma, *Spontaneous fission and competing ground state decay modes of actinide and transactinide nuclei*, Phys. Rev. C 96 (2017), 054307.
[3] G. Sawhney, K. Sandhu, M. K. Sharma, and R. K. Gupta, *Role of nuclear deformations and proximity interactions in heavy particle radioactivity*, Eur. Phys. J. A 50 (2014), 175.
[4] G. Sawhney, M. K. Sharma, and R. K. Gupta, *Role of higher-multipole deformations in exotic ^{14}C cluster radioactivity*, Phys. Rev. C 83 (2011), 064610.
[5] A. Kaur and M. K. Sharma, *Investigation of various decay mechanisms for $^{216}Th^*$ following the $^{32}S+^{184}W$ reaction in the range $E_{c.m.}$=118-196 MeV*, Phys. Rev. C 99 (2019), 044611.
[6] A. Kaur and M. K. Sharma, *Fine structure effect among heavy-ion induced fission fragments at near and above barrier energies*, Eur. Phys. J. A 55 (2019), 89.
[7] G. Kaur, K. Sandhu, A. Kaur, and M. K. Sharma, *Dynamics of Db isotopes formed in reactions induced by ^{238}U, ^{248}Cm and ^{249}Bk across the Coulomb barrier*, Phys. Rev. C 97 (2018), 054602.
[8] E. Rutherford and T. Royds, *XXIV. Spectrum of the radium emanation*, Phil. Mag. 16 (1908), 313.
[9] G. N. Flerov and K. A. Petrzhak, *Spontaneous fission of uranium*, Phys. Rev. 58 (1940), 275.
[10] H. J. Rose and G. A. Jones, *A new kind of natural radioactivity*, Nature (London) 307 (1984), 245.
[11] V. M. Strutinsky, *Shell effects in nuclear masses and deformation energies*, Nucl. Phys. A 95 (1967), 420.
[12] R. K. Gupta, N. Singh, and M. Manhas, *Generalized proximity potential for deformed, oriented nuclei*, Phys. Rev. C 70 (2004), 034608.
[13] R. K. Gupta *et al.*, *Optimum orientations of deformed nuclei for cold synthesis of superheavy elements and the role of higher multipole deformations*, J. Phys. G: Nucl. Part. Phys. 31 (2005), 631.
[14] N. J. Davidson, S. S. Hsiao, J. Markram, H. G. Miller, and Y. Tzeng, *A semi-empirical determination of the properties of nuclear matter*, Nucl. Phys. A 570 (1994), 61c.
[15] M. Balasubramaniam, R. Kumar, R. K. Gupta, C. Beck, W. Scheid, *Emission of intermediate mass fragments from hot $^{116}Ba^*$ formed in low-energy $^{58}Ni+^{58}Ni$ reaction*, J. Phys. G: Nucl. Part. Phys. 29 (2003), 2703.
[16] B. B. Singh, M. K. Sharma, R. K. Gupta, *Decay of $^{246}Bk^*$ formed in similar entrance channel reactions of $^{11}B+^{235}U$ and $^{14}N+^{232}Th$ at low energies using the dynamical cluster-decay model*, Phys. Rev. C 77 (2008), 054613.
[17] G. Audi, A. H. Wapstra, C. Thiboult, *The AME2003 atomic mass evaluation:(II). Tables, graphs and references*, Nucl. Phys. A 729 (2003), 337.
[18] P. Möller, J. R. Nix, W. D. Myers, W. J. Swiatecki, *Nuclear ground-state masses and deformations*, At. Data Nucl. Data Tables 59 (1995), 185.
[19] W. Myers and W. J. Swiatecki, *Nuclear masses and deformations*, Nucl. Phys. 81 (1966), 1.
[20] A. S. Jensen and J. Damgaard, *Shell effects in a paired nucleus for finite excitation energies*, Nucl. Phys. A 203 (1973), 578.
[21] H. Kröger, W. Scheid, *Classical models for the mass transfer in heavy-ion collisions*, J. Phys. G: Nucl. Phys. 6 (1980), L85.
[22] G. Royer and J. Mignen, *Binary and ternary fission of hot and rotating nuclei*, J. Phys. G: Nucl. Part. Phys. 18 (1992), 1781.
[23] M. Greiner, W. Scheid, *Radioactive decay into excited states via heavy ion emission*, J. Phys. G 12 (1986), L229.
[24] E. K. Hyde, *Astatine and francium*, Journal of Chemical Eduction 36 (1959), 1.
[25] G. Audi, O. Bersillon, J. Blachot, and A. H. Wapstra, *The NUBASE evaluation of nuclear and decay properties*, Nucl. Phys. A 729 (2003), 3.

[26] G. Sawhney, M. Kaur, M. K. Sharma and R. K. Gupta, *Theoretical study of odd-mass Fr isotopes using the collective clusterization approach of the dynamical cluster-decay model*, Phys. Rev. C 88 (2013), 034603.

School of Physics and Materials Science, Thapar Institute of Engineering and Technology, Patiala-147004, Punjab, India
Email address: msharma@thapar.edu

School of Physics and Materials Science, Thapar Institute of Engineering and Technology, Patiala-147004, Punjab, India
Email address: amanganday@gmail.com